Egyptian Computer Science Journal Vol. 37 No. 6 September 2013 ISSN-1110-2586

An Efficient Virtual-Work Based Trajectory Estimation Model for a Skid Steering Mobile Robot Incorporating Free Wheels

Abeer M.Mahmoud[1] and Tokuji Okada[2]

[1]Ain Shams University, Cairo, Egypt
[2]Niigata University, Niigata, Japan
abeer_f13@yahoo.com , okada@eng.niigata-u.ac.jp

Abstract

In general, the basic research areas in robotics are mapping, controlling, planning and localization. Usually, the robot creates a map of the environment, then uses this map to localize itself and plans the reference objects for its movements. The controller is designed to efficiently move it to its target. However, accomplishing the controller mission in specific requires an accurate estimation of the robot trajectory to be able to set right control parameters. This paper presents an efficient virtual-work based trajectory estimation model for a skid-steering mobile robot (SSMR) incorporating free wheels on uneven but smooth ground with different ground properties and distributed loads on wheel axes. This model is an extension of our previously published trajectory estimation model to apply not only to four-wheel-drive skid steering robot (SSRs), but also to general SSRs having decreased driving wheels either intentionally or unexpectedly. Also, the extension of our work includes a different commercial small four wheels mobile robot, named GAIA-1a, to demonstrate and verify the results. Actually, we formulate a mathematical expression in terms of virtual work for evaluating the energy cost of all the wheel motions with skidding and slipping under the condition that each wheel is always in contact with the ground via a pivot suspension structure. Minimization of the expression for virtual work results in a unique solution for the new position of the robot after small movement of the wheels. Further, by iterating we calculate a continuous trajectory which is an important result for assigning powered wheel velocities for self-navigation. The demonstrated trajectories of the test robot confirm the validity and efficiency of our method.

Key Words: *Mobile Robot; Skid Steering, Trajectory Estimation; Motion Analysis, Simulation.*

1. Introduction

The basic research areas in robotics are mapping, controlling, planning and localization. Usually, the robot creates a map of the environment, then uses this map to localize itself and plans the reference objects for its movements. The controller is designed to efficiently move it to its target. However, accomplishing the controller mission in specific requires an accurate estimation of the robot trajectory to be able to set right control parameters [1]. For wheeled mobile robots (WMRs), most studies that have been conducted, assume that their wheels satisfy a nonslip and nonskid conditions, however, in reality, tires deform while steering, thus violating both these assumptions. Actually, skid-steering is a widely used locomotion mechanism for mobile robots. Therefore, implementing an exact model with a practical control scheme is important for the study of wheel behavior. A differential angular velocity

between the two sided of a robot determines the steering of skid-steering mobile robots (SSMRs). In particular, a differential gearing system is beneficial for adjusting differential angular velocities without using steering mechanisms. A robot equipped with such a gearing system and free casters will move without sliding or skidding. A kinematic approach for analyzing tracked mobile robots has previously been proposed [2]. However, the SSMRs in that study are characterized by all skidding wheels using ground-wheels interaction and skidding effect. Meanwhile, stable motions of SSMRs are formulated in [3, 4]. A 4WD skid-steering EV has been developed in which the available torque is distributed to each wheel in order to execute the driver's commands [5]. Integrated estimation of WMR motion in the presence of wheel skidding and slipping has also been discussed [6]. In another study, a kinematic model applied to the control of an SSMR resulted in improved stability regulation and trajectory tracking in both position and orientation [7].

Skid-steer vehicles (SSVs) require increased power when cornering since turning requires an increased force to be exerted by the steering mechanism [8, 9]. In addition, SSVs show markedly higher tire wear compared with Ackermann steered vehicles because of the relatively high values of friction encountered during skidding and slipping when steering. However, the absence of an explicit steering assembly makes four wheel drive SSVs (4WDSSVs) mechanically robust and able to move on rough terrain with toughness and good maneuverability by controlling the wheels simply by varying their angular velocity, for example, as an all-terrain response vehicle (ATRV). Skid-steering based on dynamic models for real-time motion control of n-wheel driving SSMRs may be costly. Therefore, it is more practical and effective to control wheel pairs at opposite sides of the nWDSSMRs with differential velocity inputs.

This paper extends our previous trajectory estimation method [10] to apply not only to four-wheel-drive SSRs, but also to general SSMRs having decreased driving wheels either intentionally or unexpectedly. This paper focuses on various wheel driving arrangements, some of which include free wheels. Experimental data gathered from an actual robot to verify the method for estimating motion trajectories are presented. The rest of the paper is organized as follow, Section 2, introduce nomenclature. The model of the robot and different wheel driving axel arrangements are in section 3. Section 4, analyzes the skidding and slipping behaviors of a 4WSSMR. The robot trajectory estimation is presented in section 5. The simulation results and real demonstration experiments are in sections 6 and 7, respectively. Section 8, concludes the paper.

2. Parameters Definition

The paper uses many mathematical symbols and parameters for the explanation of kinematics and dynamics modeling of the skid steering robot, in addition to the estimation algorithm that requires a set of parameterized controls to encode the motion of the robot, in the following, there exist the definition of these parameters.

(a,b) : X and Y components of the robot center on the planes of λ_o and λ. (a_e, b_e) shows a small linear displacement

I : Subscript related to the wheel position ($i = 1-5$)

D_i : Translational wheel displacement, i.e., $\overline{P_i P_i'}$

L_i : Expected rolling distance of the wheel within Δt

A_i : Wheel tread area (width; t_{ai}, length; t_{bi})

L : Body size (body length; L_h, body width; L_w)

P_{i0} : Initial wheel position (x_{i0}, y_{i0}, z_{i0}) on ζ_0

P_i' : Actual wheel position (x_i', y_i', z_i') on ζ after a small wheel rotation

P_{si} : Expected wheel position (x_{si}, y_{si}, z_{si}) on ζ when the wheel rolls forward by a small angular displacement

P_c : Geometric center of the robot

P_g : Center of mass of the robot

P_5 : Imaginary point where the resultant force at P_1 and P_2 operates

P_6: : The point where the axis η crosses the vertical plane including P_1 and P_2

P_7 : Vertical projection of P_g on the plane ζ

Ri : Wheel radius

U_i : Supposed virtual distance, i.e., $\overline{P_i' P_{si}}$

W_{i0} : Load at the wheel contact on ζ_0 (i = 1−5,7)

W_i : Load at the wheel contact on ζ (total load, Wt

α : Angular shift of a wheel from an initial direction. α_e shows a small displacement

H : Axis of a pivot suspension; virtual body axis extending straight forward parallel from P_c internally around which the front body part is compliant and twist in order to have four wheels in contact with an irregular terrain

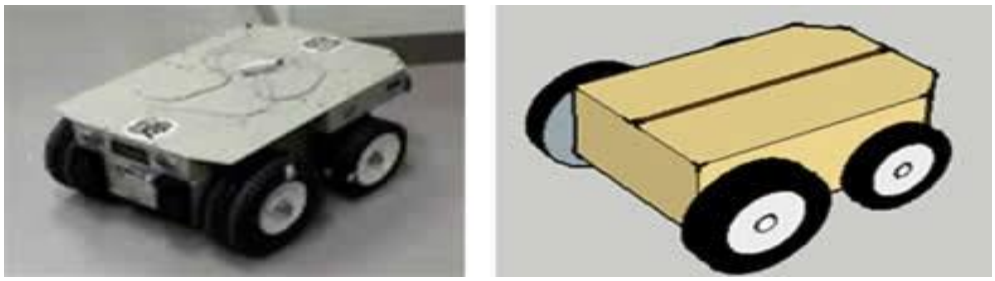

Fig. 1. the GAIA mobile Robot

Φ : Twist angle of the front body part around η

θ_r : Wheel rotation angle (small increment, $\Delta\theta_r$)

Θ_s : Inclination angle of the ground surface

μ_i : Friction coefficient (static; μ_{si}, dynamic; μ_{di})

v_i : Linear speed of a wheel movement

ω_i : Angular velocity of i-th wheel (left; ω_l, right; ω_r)

Λv : Ratio of ω_l to ω_r (= v_r/v_l)

ζ_0 : X_0-Y_0 plane; horizontal home ground of the robot before the coordinate transformation

Z : X−Y plane; actual ground surface generated after the coordinate transformation of Σ_0 with θs around the X_0 axis

Σ_0 : Coordinate system of the horizontal home ground

Σ : Coordinate system of the ground inclined by θs.

3. Model of the Robot

The subject of this paper is commercially small four-wheeled mobile robots, named GAIA-1a, see Fig 1. The specifications of GAIA-1a are presented in the following

L_h	:	53cm(overall), 48cm(between axes)
Lw	:	36cm(overall), 31cm(between wheels)
Wheel	:	front(solid); radius = 8.7cm, rear(nylon); radius = 10.8cm
Tread	:	front; ta = 7.5cm, tb = 3.0cm, rear; ta = 8.0cm, tb = 4.5cm
μ_i	:	p − tile; 0.44(front), 0.51(rear). wood; 0.56(front), 0.79(rear)
Driver	:	Vista board, Battery(24Ah, 12V), 100ppr, Max. speed; 2.8km/h
Sensor	:	Encoder; 100 ppr, Marker position; 32.5cm(Pmf), − 28cm(Pmb)

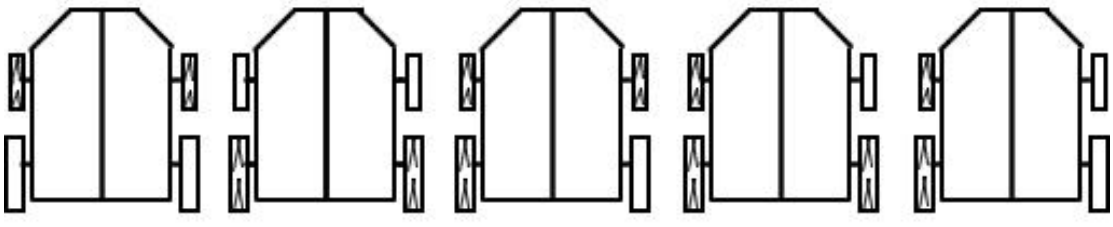

Fig. 2. Top view of SSWMRs illustrating various driving wheel arrangements including free wheels

3.1 Wheel Driving Axel Arrangements

Wheeled robots move whenever there is at least one wheel driving wheel. Multi-wheeled vehicles may be assembled with wheels of different sizes, and some may be driving while others are not. Some wheels may roll freely without necessitating drive power by means of a link, chain, or belt. Steam locomotives, for example, make use of such a link. In skid-steering mobile robots and vehicles, arrangements where all the wheels are powered, e.g., 4WD are the most effective for generating large traction forces. However, unbalanced arrangements can occur in unexpected conditions. Various wheel arrangements (excluding the 4WD) are shown in Fig.1. Here, rectangles with arrow-like hatches show powered wheels and their directions of movement, and rectangles without hatches show free wheels. Arrangements (1) and (2) are FWD (Front WD) and RWD (Rear WD), respectively. These balanced arrangements are popular when an explicit steering mechanism is used. The unbalanced arrangements (3) and (4) occur in unexpected conditions. We refer to them as *FL3WD* (Front-Left 3WD) and *RL3WD* (Rear-Left 3WD), respectively. Similarly, *FR3WD* (Front-right 3WD) and *RR3WD* (Rear-right 3WD) are also considered.

These 3WD arrangements replace a driving wheel with a free wheel and operate better than FWD and RWD in steering performance. Arrangement (5) in Fig.2, LWD (Left WD) and similarly RWD (Right WD), which is not shown in the figure will rarely happen. In this paper, we do not consider special arrangements such as a crawler or a robot in which the powered wheels are located diagonally.

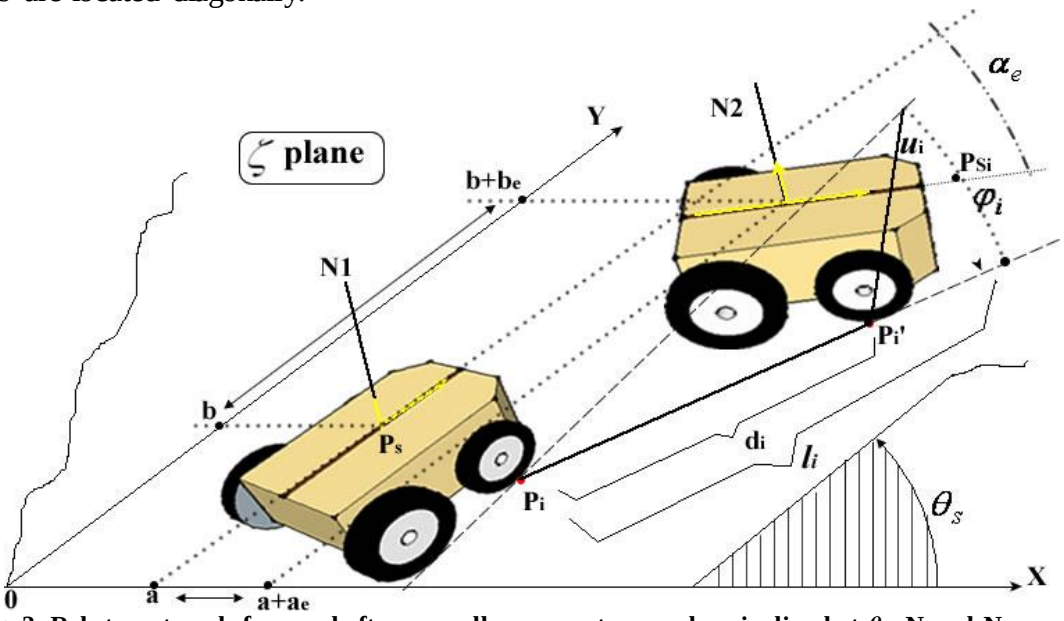

Fig. 3. Robot posture before and after a small movement on a slope inclined at θs. N_1 and N_2 are the normal to the robot platform

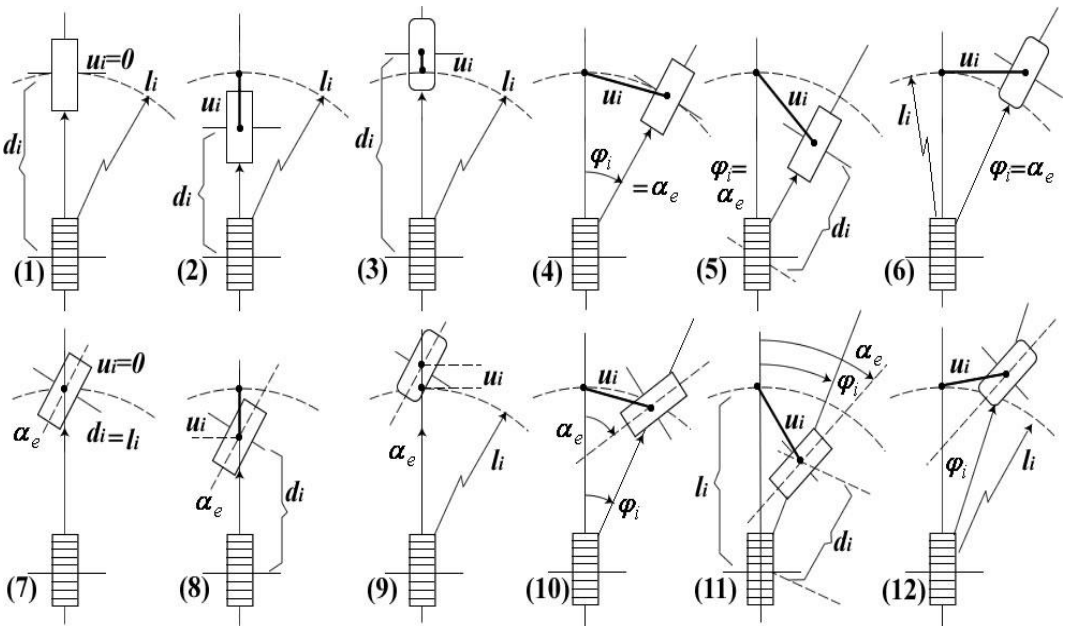

Fig. 4. Possible patterns of skidding and slipping behaviors as a mixture of twists and translations. Unhatched and hatched rectangles show wheel positions with postures before and after small motion, respectively

4. Analyses of Skidding and Slipping Behaviors

Fig.3 shows the movement of a 4WSSMR on the slope. Suppose that each wheel skids and slips while rolling. Then, the possible wheel behaviors can be categorized into eleven patterns shown in Fig.4. Each pattern is not determined locally, because the motion is interactive among the four wheels (see Fig.3). Since the robot trajectory cannot be expressed using a closed algebraic expression, we seek to solve for a continuous path by iteratively solving for incremental changes in the robot's position caused by small changes to the driving wheel angles.

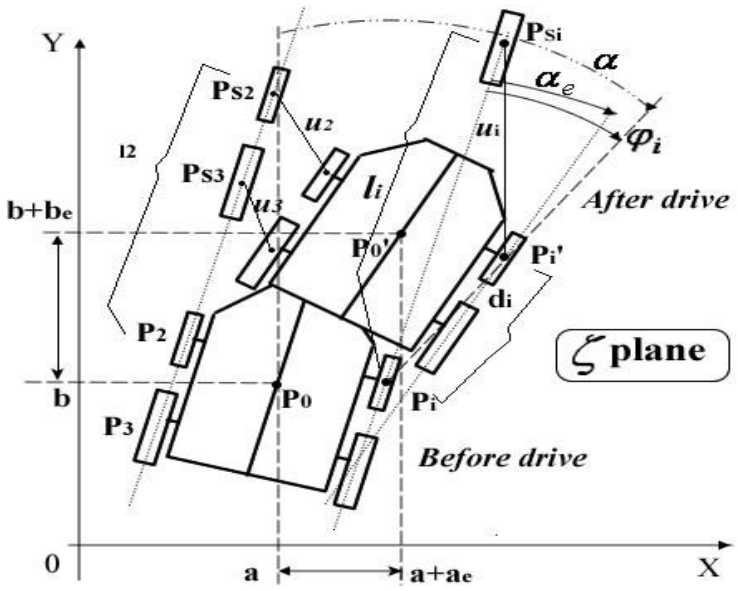

Fig. 5. Illustration of virtual distance U_i connecting Psi and P

4.1 Transformation of Wheel Tread Position

Suppose that the robot stands on the plane ζ_0 by aligning P*c* on the Z_o-axis and having the robot point toward the Y_0 direction. In Addition, imagine that each wheel rolls a distance l_i which is equal to $R_i\omega_i\Delta t$ when drive power is supplied. Then, $P_{si}(x_{si}, y_{si}, z_{si})$ in the system Σ is combined with $P_{i0}(x_{i0}, y_{i0} + l_i, z_{i0})$ in the system Σ_0 (Fig.5). In fact, l_i is zero when the robot locks a wheel *i* from rolling. These relations are written in matrix form as given below:

$$\begin{bmatrix} x_{si} \\ y_{si} \\ z_{si} \\ 1 \end{bmatrix} = Rot(X, \theta_s)Trans(a, b, 0)Rot(Z, -\alpha) \begin{bmatrix} x_{i0} \\ y_{i0} + l_i \\ z_{i0} \\ 1 \end{bmatrix} \quad (1)$$

Similarly, after each wheel rolls independently on the plane ζ, $P_i'(x_i', y_i', z_i')$ is combined with $P_{i0}(x_{i0}, y_{i0}, z_{i0})$ using the variables (a_e, b_e) and α_e. Moreover, $z_{i0}' = 0$ holds for the same plane ζ_0. Accordingly,

$$x_i^{'} = x_{i0}\cos(\alpha+\alpha_e) + (y_{i0}+l_i)\sin(\alpha+\alpha_e) + a + a_e \quad (2)$$

$$y_i^{'} = \{-x_{i0}\sin(\alpha+\alpha_e) + (y_{i0}+l_i)\cos(\alpha+\alpha_e) + b + b_e\}\cos\theta_s - z_{i0}\sin\theta_s \quad (3)$$

$$z_i^{'} = \{-x_{i0}\sin(\alpha+\alpha_e) + (y_{i0}+l_i)\cos(\alpha+\alpha_e) + b + b_e\}\sin\theta_s - z_{i0}\cos\theta_s \quad (4)$$

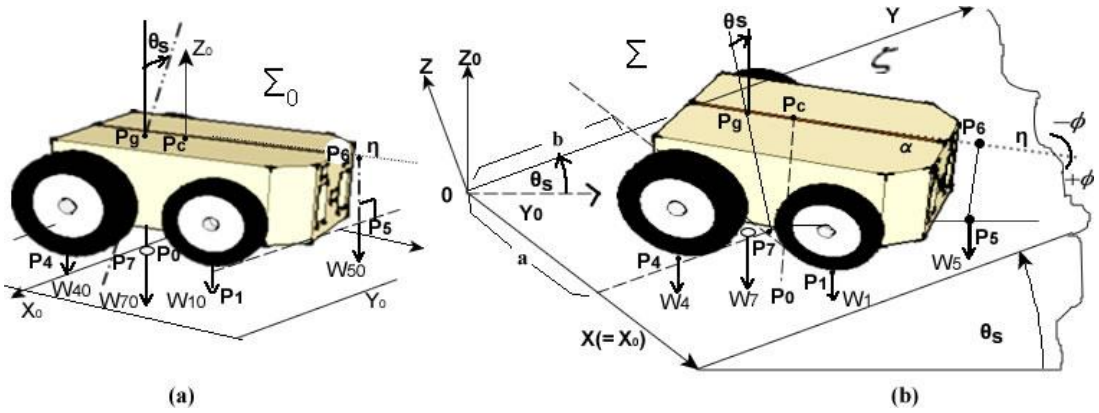

Fig. 6. Robot standing on the plane ζ_0 (a) is transferred to the position on the plane ζ (b) after a coordinate transformation with the parameters (a,b) and α.

Concerning the weight distribution W_i, it is difficult to determine the load at each wheel tread uniquely because, in general, all four wheels are in contact with the ground, our robot model is compliant, resulting in four wheels always being in contact with the ground, we assume that the front and rear parts of the robot body are able to twist freely around the η-axis that extends straight forward from Pc in the robot body as a front pivot suspension (Fig.6). We consider the line $\overline{P_5P_6}$ as making a virtual wheel touch on the ground at P_5 so that W_t is shared among the three points P_3, P_4 and P_5. Then, we distribute the weight W_5 at P_5 between W_1 and W_2 at P_1 and P_2, respectively. This is our method for distributing the instantaneous weight to all four wheels in contact with the ground. Actually, a static analysis introduces the following equilibrium relationships:

$$W_t = W_3 + W_4 + W_5 \quad (5)$$

$$W_5 = W_1 + W_2 \quad (6)$$

$$0 = \overrightarrow{P_gP_6} \times W_5 + \overrightarrow{P_gP_3} \times W_3 + \overrightarrow{P_gP_4} \times W_4 \quad (7)$$

$$0 = x\overrightarrow{P_6P1} \times W1 + (1-x)\overrightarrow{P_6P_2} \times W_2 \quad (8)$$

where the parameter χ is defined as a coefficient related to $\pm\phi$ (see Fig.6). This is important when the ground surface is not flat and the load balance between W_1 and W_2 varies.

In fact, the robot body compliance determines $\pm\phi$ on uneven ground. Therefore, we write $\chi = 0.5+K_0\phi$, where K_0 is the twisting compliance factor of the front body. Note that χ varies in the range $0 < \chi < 1$, and takes the value 0.5 when the body can twist freely, i.e.,

when $K_0 = 0$. By solving the independent equations (5)−(8) having 7 unknown variables, we can determine the position P_5 and weights $W_1 - W_5$ in the state described by *(a, b)* and $\alpha\,\alpha$ on the plane ζ.

4.2 Formulation of an Energy Cost Function Using a Virtual Work

Suppose that some wheels are driven independently. Then, skidding and slipping occur while the robot moves. Each wheel movement is composed of positional and angular displacements, which we call *linear sliding* and *twist sliding*. Drive power is needed to accomplish sliding, which is a combination of skidding and slipping. In addition, energy is necessary when the robot rolls up a slope. When rolling down a slope, the robot moves downward by consuming its gravitational potential energy. Therefore, the virtual work for sliding appears in the form of energy for twist sliding, linear sliding and any change in gravitational potential energy [11]. Let us suppose that E_1, E_2 and E_3 denote each of the three energy costs, respectively. Then these can be expressed by referring to Fig.5.

Suppose that each wheel in contact with the ground with a rectangular tread, and that the pressure in the area is unique, irrespective of the contact position. That is, $W_i = t_{ai}t_{bi}\,\tau$, where τ is a pressure in units of pressure. Using α_e, we obtain two expressions:

$$E_{1i} = \int_0^{\alpha_i} \int_{-t_b/2}^{t_b/2} \int_{-ta/2}^{ta/2} \mu_{di}\tau(x^2+y^2)\,dx\,dy\,d\alpha$$

$$= \mu_{di}|\alpha_e|w_i \cos\theta_s (t_{ai}^2 + t_{bi}^2)/12 \tag{9}$$

$$E_{2i} = \mu_{di}U_i c|\upsilon_i|W_i \cos\theta_s \tag{10}$$

It follows that

$$U_i c|\upsilon| = U_i c\left|U_i/\Delta t\right| = U_i^2\, c/\Delta t \equiv KU_i^2 \tag{11}$$

Where

$$U_i^2 = (x_i' - x_{si})^2 + (y_i' - y_{si})^2 + (z_i' - z_{si})^2$$

$$= a_e^2 + C_{1i}a_e\cos\alpha_e + C_{2i}a_e\sin\alpha_e + C_{3i}a_e + b_e^2 + C_{4i}b_e\cos\alpha_e + C_{5i}b_e\sin\alpha_e + C_{6i}b_e + C_{7i}\cos\alpha_e + C_{8i}\sin\alpha_e + C_{9i} \tag{12}$$

The constants $C_{1i} - C_{9i}$ are defined as

$C_{1i} = 2(x_{i0}\cos\alpha + y_{i0}\sin\alpha)$ $\quad$ $C_{2i} = -2(x_{i0}\sin\alpha - y_{i0}\cos\alpha)$

$C_{3i} = -2\{x_{i0}\cos\alpha + (y_{i0} + \_i)\sin\alpha\}$ $\quad$ $C_{4i} = C_{2i}\,C_{5i} = -C_{1i}$

$C_{6i} = -C_{2i} - 2l_i\cos\alpha$ $\quad$ $C_{7i} = (C_{1i}C_{3i} + C_{2i}C_{6i})/2$

$C_{8i} = 2x_{i0}l_i$ $\quad$ $C_{9i} = 2(x_{i0}^2 + y_{i0}^2) + l_i(2y_{i0} + li)$

Using another constant K simplifies expression (10) as follows:

$$E_{2i} = W_i \, \mu_{di} K \, U_i^2 \, \cos\theta_s \tag{13}$$

So far in our analysis, U_i^2 is assumed to be zero when the i-th wheel has no power. This free wheel is supposed to roll a distance l_j ($j \neq i$) that is generated by a neighboring powered wheel since the robot maintains its body frame nearly rigid except while twisting. However, there is some force feedback caused by the rotational friction around each wheel axis in an actual machine. Therefore, we assume that U_i^2 has a certain value proportional to the friction force, and express U_i^2 as a small value by defining a coefficient δi that is nearly equal to zero. For a powered wheel, δi is equal to 1. This consideration generalizes equation (13) as follows:

$$E_{2i} = \delta_i W_i \, \mu_{di} K \, U_i^2 \, \cos\theta_s \tag{14}$$

The exact value of μ_{di} is difficult to predict because it is subject to constant change in an actual environment. However, assuming there is a certain constant value, say e, then μ_{di} in equations (9), (10), (13) and (14) can be expressed as in [12], such that

$$\mu_{di} = (1 - e \, v_i) \, \mu_{si} \tag{15}$$

In particular, v_i as well as d_i are both small quantities in our analysis. Thus, μ_{di} is assumed to be a smaller constant than that of $\mu_{si.}$ This implies that a faster motion will be estimated using the small value of μ_i. Henceforth we use μ_i in place of μ_{di} without the risk of underestimating motion. Concerning the gravitational potential energy, it is evaluated by the following expression:

$$\begin{aligned} E_{3i} &= Wi(z_i^{'} - z_i) \\ &= W_i \sin\theta_s (C_{2i} \cos\alpha_e - C_{1i} \sin\alpha_e + 2b_e - C_{2i})/2 \end{aligned} \tag{16}$$

Finally, we can sum each energy cost to yield an expression for the total cost.

$$\begin{aligned} E_t &= \sum_{i=1}^{4} \{E_{1i} + E_{2i} + E_{3i}\} \\ &= \sum [\{(t_{ai}^2 + t_{bi}^2)/12\mu_i |\alpha_e| \cos\theta_s + \mu_i \delta_i K U_i^2 \cos\theta_s + (z_i^{'} - z_i)\} W_i] \\ &= a_e(\lambda_1 a_e + \lambda_2 \cos\alpha_e + \lambda_3 \sin\alpha_e + \lambda_4) + b_e(\lambda_5 b_e + \lambda_6 \cos\alpha_e + \lambda_7 \sin\alpha_e + \lambda_8) + \lambda_9 \cos\alpha_e + \lambda_{10} \sin\alpha_e + \\ &\lambda_{11} + \lambda_{12} |\alpha_e| \end{aligned} \tag{17}$$

where

$$\lambda_1 = K \cos\theta_s \sum_{i=1}^{4} \{\delta_i W_i \mu_i\}, \qquad \lambda_2 = K \cos\theta_s \sum \{\delta i \, W_i \mu_i \, C_{1i}\}$$

$$\lambda_3 = K \cos\theta_s \sum \{\delta_i \, W_i \mu_i \, C_{2i}\}, \qquad \lambda_4 = K \cos\theta s \sum \{\delta_i \, W_i \mu_i \, C_{3i}\}$$

$$\lambda_5 = \lambda_1, \qquad \lambda_6 = \lambda_3, \qquad \lambda_7 = -\lambda_2$$

$$\lambda_8 = \sum [W_i\{\delta_i K\mu_i \cos\theta_s C_{6i} + \sin\theta_s\}]$$

$$\lambda_9 = \sum [W_i\{\delta_i K\mu_i \cos\theta_s(C_{1i}C_{3i} + C_{2i}C_{6i}) + C_{2i}\sin\theta_s\}/2]$$

$$\lambda_{10} = \sum [Wi\{\delta iK\mu i \cos\theta sC8i - C1i \sin\theta s/2\}]$$

$$\lambda_{11} = \sum [W_i\{\delta_i K\mu_i \cos\theta_s C_{9i} + C_{6i}\sin\theta_s/2\}]$$

$$\lambda_{12} = \sum \{W_i\ \mu_i \cos\theta_s(t^2_{ai} + t^2_{bi})/12\}$$

4.3 Minimization of Virtual Work

The robot movement can be predicted by solving for the unknown parameters (a_e, b_e) and α_e. Thus, we differentiate (17) by each of these parameters since, based on the principle of virtual work, (17) is minimized when there is no energy loss except for skidding and slipping.

$$dE_t/da_e = 2\lambda_1 a_e + \lambda_2 \cos\alpha_e + \lambda_3 \sin\alpha_e + \lambda_4 = 0 \quad (18)$$

$$dE_t/db_e = 2\lambda_5 b_e + \lambda_6 \cos\alpha_e + \lambda_7 \sin\alpha_e + \lambda_8 = 0 \quad (19)$$

$$dE_t/d\alpha_e = -(\lambda_2 \sin\alpha_e - \lambda_3 \cos\alpha_e)a_e - (\lambda_6 \sin\alpha_e - \lambda_7 \cos\alpha_e)b_e$$
$$-(\lambda_9 \sin\alpha_e - \lambda_{10}\cos\alpha_e - \lambda_{12}) = 0 \quad (20)$$

Substituting *ae* in (18) and *be* in (19) into (20) generates a single equation with only one unknown parameter α_e. However, it is difficult to solve the resulting fourth order equation for α_e, algebraically. Therefore, we assume that $\alpha_e \approx 0$ so that $\sin\alpha_e \approx \alpha_e$, $\cos\alpha_e \approx 1$ and $\alpha_e{}^2 \approx 0$. This reasonable approximation simplifies the solution such that

$$a_e = -(\lambda_2 \cos\alpha_e + \lambda_3 \sin\alpha_e + \lambda_4)/(2\lambda_1) \quad (21)$$

$$be = -(\lambda_6 \cos\alpha_e + \lambda_7 \sin\alpha_e + \lambda_8)/(2\lambda_5) \quad (22)$$

$$\alpha_e = \lambda_1\{\lambda_7\lambda_{68} - 2\lambda_5(\lambda_{10} + \lambda_{12})\} + \lambda_3\lambda_5\lambda_{24} \,/\, \lambda_1\{\lambda_6\lambda_{68} - 2\lambda_5\lambda_9 - \lambda_7{}^2\} + \lambda_2\lambda_5\lambda_{24} - \lambda^2{}_3\lambda_5 \quad (23)$$

where λ_{24} and λ_{68} denote $\lambda_2+\lambda_4$ and $\lambda_6+\lambda_8$, respectively. Note that λ_{11} is a constant and disappears from (21)−(23). The next robot position is introduced repeatedly by replacing the old parameters (a, b) and α with the new ones ($a+a_e$,$b+b_e$) and $\alpha + \alpha_e$ to connect position histories in order to form a continuous trajectory.

5. The Trajectory Estimation Algorithm

The robot's motion is simulated by evaluating each step in the following procedure.

1. Assign the robot's dimensional specifications L_h, L_w, R_i, W_t, A_i, μ_i, η, θ_s, ω_i and $\Delta\theta_r$. Values for each of these parameters are given in the experiment discussed in Section 6. In normal conditions, the constants K and χ are 1.0 and 0.5, respectively; however, they are not limited to these values depending on the robot's specifications and unevenness of the ground.

2. Locate the robot on the home ground to assign $P_{i0}(i = 1-4)$ on the plane ζ_0. Then assign $l_i(i = 1-4)$ and apply the coordinate transformation using the initial parameters a, b, α and $l_i(i = 1-4)$ to calculate $P_{si}(i = 1-4)$.

3. Similarly, locate the robot on the home ground again and apply the coordinate transformation using the parameters $(a+a_e, b+b_e)$ and $\alpha + \alpha_e$ to calculate the next incremental position $P_{si}(i = 1-4)$ on the plane ζ. If the i-th wheel is free, then assign a value for δ_i by considering the wheel resistance, and also assign a value for l_i equal to that of the driving wheel of the same side on the front or rear. If all the wheels on one side are free, then use the value of l_i on the other side for the front or rear. Set each l_i to be the same value as that of the powered wheel if only one wheel is powered.

4. Calculate the wheel load $W_i(i = 1-4)$ through the weight W_5 which is the intrinsic weight operating at the virtual wheel tread at P_5.

5. Calculate the parameters $C_{1i} - C_{9i}$ to determine the square of the virtual distance U_{2i}

6. Calculate the parameters $\lambda_1 - \lambda_{10}, \lambda_{12}, \lambda_{24}$ and λ_{68} to evaluate E_t.

7. Solve the equation to obtain (a_e, b_e) and α_e, and determine the position $P'_i(i = 1-4)$ on the plane ζ for the next desired position after incrementing θ_r with $\Delta\theta_r$.

8. Save the incremental position as a history along the trajectory. Then repeat the procedure from step 2. by replacing the parameters (a, b) and α, with $(a+a_e, b+b_e)$ and $\alpha + \alpha_e$, respectively.

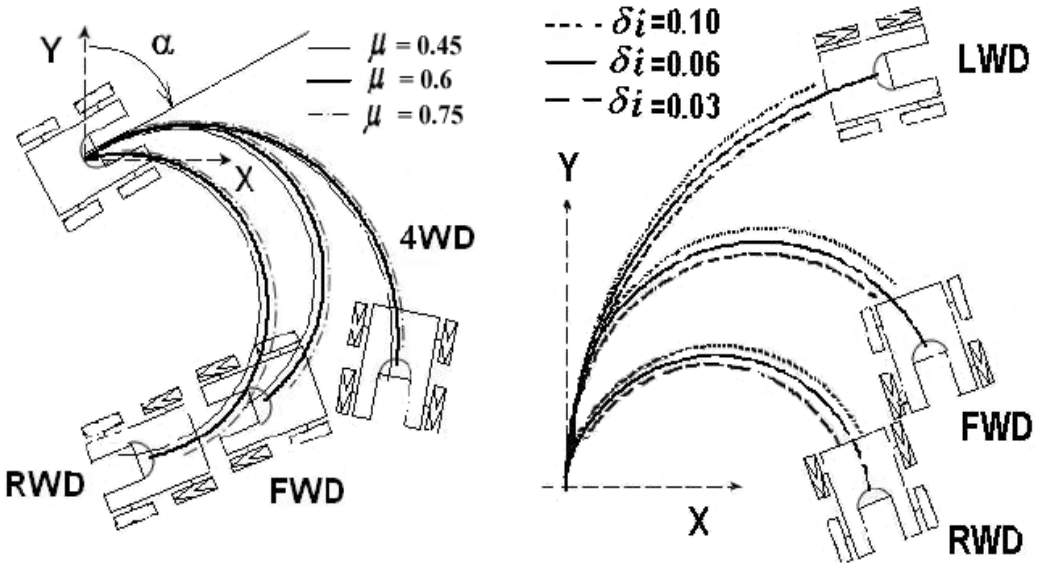

Fig. 7. (a)Right turn trajectories influenced by μ_i on horizontal ground within α = 60, (b)Changes in trajectory depending on the free-wheel resistance δ_i for FWD, RWD and LWD configurations on horizontal ground.

6. Motion Simulation Using Generated Trajectories

Traversing a straight path, steering by turning and pinning are demonstrated and compared while studying the effects of the following factors with each of the powered wheel arrangements shown in Fig.2.

- Ground friction coefficient
- Powered wheel arrangement
- Free − wheel resistance
- Wheel tread area
- Shifting of robot's center of mass

Let us suppose that the robot turns with $0.45 \leq \mu_i \leq 0.75$ and $\lambda v = 2.0$. The coefficients for assigning the resistance in FWD and RWD are $\delta_3 = \delta_4 = 0$ and $\delta_1 = \delta_2 = 0$, respectively. Then the circular trajectories for 4WD, FWD, and RWD configurations are shown in Fig.7(a). The starting direction α is 60◦ and 0◦, in (a) and (b), respectively. In each case, μ_i and tread are 0.6 and (t_{ai}, t_{bi}) = (1cm, 2cm), respectively. The scale is 1/44.2. For clarity, only the final state of the robot is sketched. It is clear that the direction of the robot shifts away from starting direction in each case. To study how the trajectories are influenced by the free wheel resistance, we simulate the motion for FWD (λv = 2), RWD (λv = 2) and LWD by assigning different values for δ_i in (17). In particular, $\delta_3 = \delta_4$ in FWD, $\delta_1 = \delta_2$ in RWD and $\delta_1 = \delta_4$ in LWD are assigned to be 0.03, 0.06 and 0.10, respectively. Fig.7(b) shows the simulated trajectories. All the left−side−powered angular velocities are equal in the three arrangements. Other conditions are maintained constant while turning, that is, for instance, μ_i = 0.6, (t_{ai}, t_{bi}) = (1cm, 2cm) and χ = 0.5 are maintained. The results clearly show that each trajectory has a circular shape with a curvature that decreases when the resistive force increases. These results

seem reasonable based on the common sense that a turn becomes more difficult with increasing resistance.

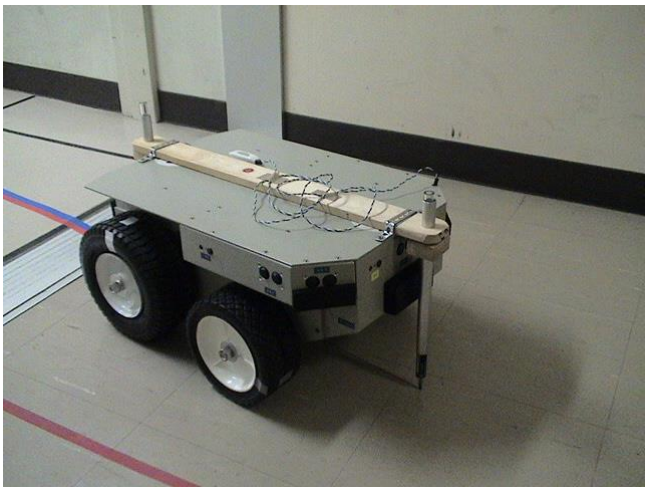

Fig. 8. the robot GAIA-1a with two places for attaching pens to draw trajectories

7. Experimental Verification

We prepared three test grounds for demonstrating robot motion. The first ground surface is a flat p-tile office floor. The second test ground is a flat wooden floor that is constructed by laying pieces of plywood of size 180 cm × 90 cm × 1.2 cm tightly on top of the p-tile floor. The third test ground is an inclined floor made of wood with a flat area of 2.7 × 3.6 m^2 inclined by θ_s = 6◦. We refer to the three test floors as the *p-tile floor*, *wooden floor* and *wooden slope*. We affixed 2-cm wide black tape to make 1m × 1m grids on each floor. For these experiments, we used a commercially available robot, the GAIA-1a whose specifications are presented in section 2. Note that the friction coefficients are dependent on the combination of the material of the floor and that of each wheel. In order to collect trajectory form and size while the robot GAIA-1a moves, we attached a tool for holding pen marker moves up and down freely and draw its bottom position on the ground directly with the effect of its own weight. Fig.8 shows the positions of those markers.

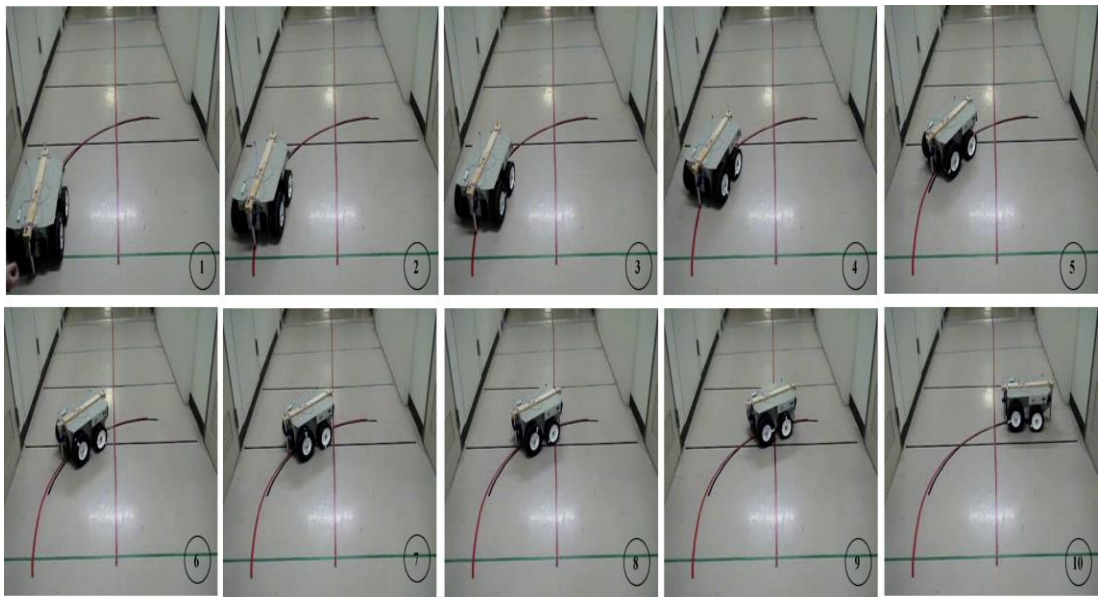

Fig. 9. Demonstration of GAIA-1a robot while turning on a p-tile flat ground.

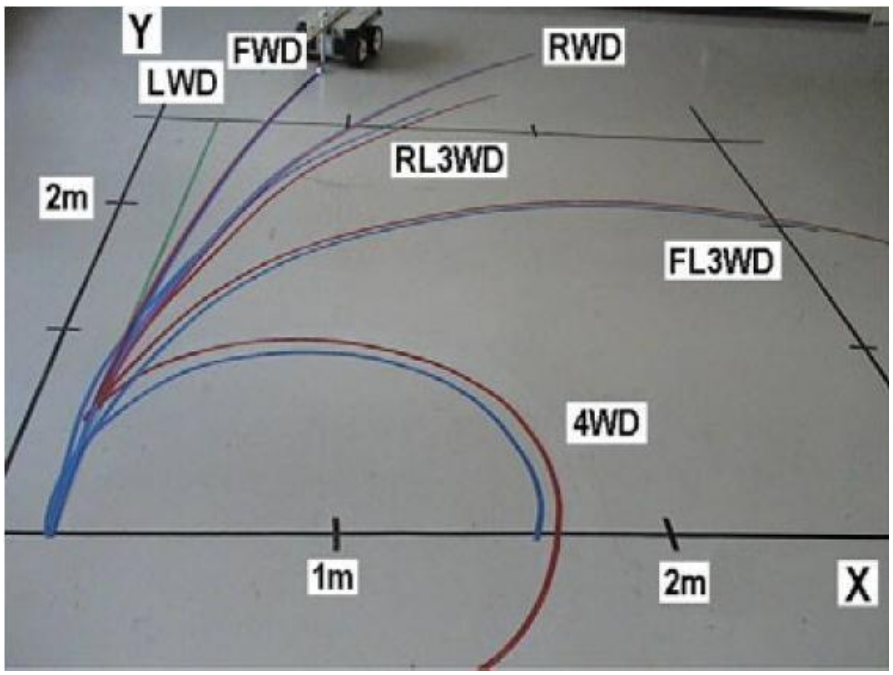

Fig. 10. Trajectories of P_{mf} and P_{mb} traced by the GAIA-1a robot during turning under 4WD, FWD, RWD, FL3WD and LWD configuration with $\alpha = 0^{o}$

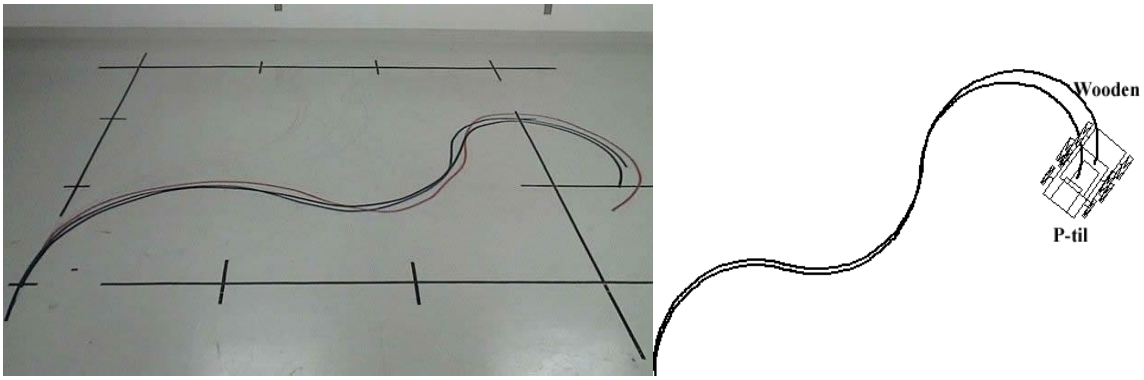

Fig 11: simulated and experimental trajectories of curvature motion

7.2 Turning

Fig.9 shows the demonstration sequence during turning of GAIA-1a on a p-tle flat ground numbered in 1 to 10 for ease of visualizing the experiment. Also, drawn as the sets of P_{mf} and P_{mb}, Fig.10 shows the trajectories produced using 4WD, 3WD and 2WD powered driving arrangements on the p-tile floor. While turning right, the robot faces the centrifugal direction in RWD and RL3WD, but the centripetal direction in 4WD, FWD and FL3WD. This results in the fact that the trajectories following P_{mf} appear inside of those following P_{mb} trajectories. By comparing the trajectories in Fig.10, we confirm that 4WD is capable of making the tightest turn. Also, Fig. 11, shows simulated and experimental trajectories of continuous curvature motion, on a p-tile and a wooden flat ground, which confirm the validity of the estimation algorithm.

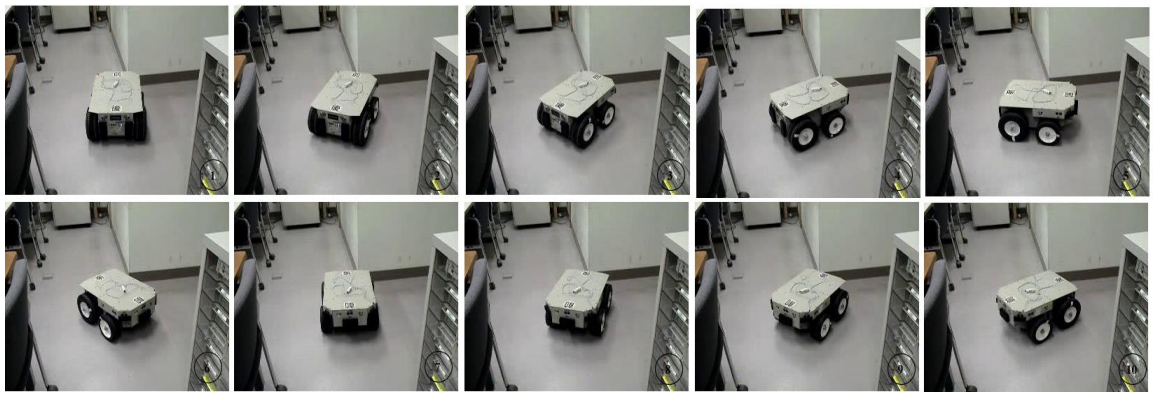

Fig 12: GAIA-1demonstration of spinning right on the p-tile ground

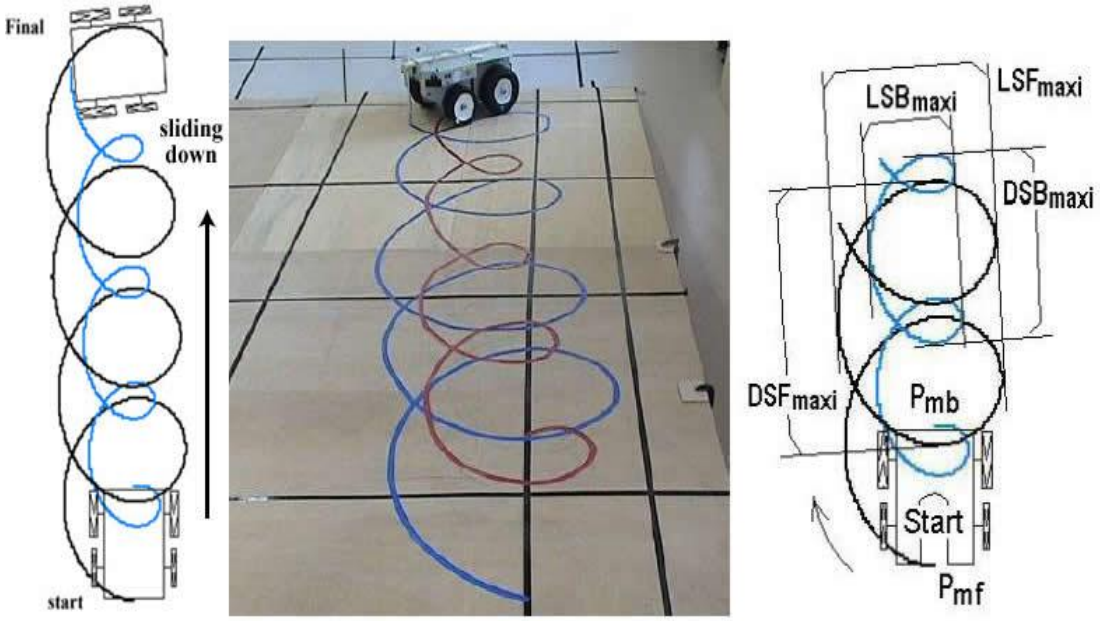

Fig. 13. Simulated and experimental trajectories of spin motion from the high-leveled bottom to low-leveled top by the GAIA-1a. Simulation results, experimental results and definition of measurement variables are shown on the left, center, and right, respectively.

Table 1. Comparison of simulated and experimental trajectories for the GAIA-1a robot spinning down a wooden slope.

	Simulated	**Experimental**				
Length(mm)	***Average***	***First***	***Second***	***Third***	***Average***	***Error(mm)***
LSF_{max}	816.8	760.0	843.4	805.6	803.0	+13.8
DSF_{max}	1172.7	1191.5	1243.2	1269.2	1234.6	−61.9
LSB_{max}	449.6	460.0	441.4	439.0	446.8	+2.8
DSB_{max}	812.9	819.7	791.7	1100.0	903.8	−90.9

7.3 Spinning

Fig.12 shows the demonstration sequence during spinning of GAIA-1a on a p-tle flat ground numbered in 1 to 10 for ease of visualizing the experiment. Spinning motion was studied also, by having the GAIA-1a robot move gradually down the wooden slope by 4WD. Fig.8 shows the experimental trajectories produced by P*mf* and P*mb* after the motion was complete along with the simulated trajectory under the aforementioned specifications and the supposition that $\chi = 0.5$. Graphically comparing the simulation results with the experimental results indicates a very close mapping between the two. Any error between the simulation and the experimental results may be due to the surface imperfections of the wood on the slope.

To evaluate the correctness of the simulation quantitatively, however, the simulation results are compared with the experimental results by defining several variables of interest to measure as shown on the right-hand side of Fig.13. These variables include DSF_{max}; the maximum span within the front marker trajectory during decent, and LSF_{max}; the maximum lateral span within the front marker trajectory. DSB_{max} and LSB_{max} are similarly defined for the back marker trajectory. These four measurements are taken three times consecutively in the experiment. Table 1 shows the simulated and experimental data for these measurements. From the table, it is clear that descending span is larger than the lateral span in both the simulated and experimental results. Positional error between the experimental and simulation data is less than 10 cm and it appears as stretching the descending span in the experimental data as compared to a smaller simulated span. This discrepancy may be caused by a decrease in the value of μ_i in the direction of decent, which would tend to stretch the span. In other words, the robot gains linear velocity as it traverse down the slope due to acceleration of the robot that is not unaccounted in our simulation model because the value of μ_i is constant.

8. Conclusion

The paper presented an estimation model as an extension of our previously published trajectory estimation model to apply not only to four-wheel-drive skid steering robot (SSRs), but also to general SSRs having decreased driving wheels either intentionally or unexpectedly. Also, the extension of our work includes a different commercial small four wheels mobile robot, named GAIA-1a, to demonstrate and verify the results.

The paper proposed a trajectory estimation method for four-wheeled SSMRs and SSVs configured with a combination of powered and non-powered wheels. A pivot suspension structure made it possible for all the wheels to be in contact with uneven ground by partially twisting the robot body. We formulated an energy cost function for expressing the effect of skidding and slipping including the change in gravitational potential energy.We specifically focused on different wheel arrangements, the resistive force of non-powered (i.e., free) wheels, the influence of the friction coefficient of the ground surface, the instantaneous load distribution to each wheel, the wheel tread area, and the slope of the ground. Minimizing the sum of the energy costs using the principle of virtual work resulted in an iterative solution for a continuous trajectory. We successfully depicted continuous trajectories as simulated graphical plots for cases in which a robot moves straight forward/ backward, turns and spins.

We conducted experiments with GAIA-1a robot. Measured trajectories from having the robot execute motions on three different types of floors showed excellent agreement with the simulated trajectories both size and shape. In future work, we intend to develop a self-navigation system that determines the exact value of λv automatically by considering environmental ground properties using sensor data (for instance, slope angle as determined by a two-axis gravity sensor) so that a driver can maneuver using a joystick in an outdoor environment with the same feeling as in an indoor environment.

References

[1] K.Kanjanawaniskul, "Motion control of a wheeled mobile robot using model predictive control: A Survey", J. of KKU, vol.17, no.5, pp.811-837, 2012.

[2] Martinez, J.L., Mandow, A., Morales, J., Pedraza, S., Garcia-Cerezo, A.: "Approximating kinematics for tracked mobile robots". Int. J. of Robotics Research , vol.24, no.10, pp.867–878, 2005

[3] Kozlowski, K., Pazderski, D.: "Practical stabilization of a skid-steering mobile robot – A kinematic-based approach", In: Proc. IEEE 3rd Int. Conf. on Mechatronics, pp. 519–524, 2006.

[4] Wang, D., Low, C.B.: Modeling and analysis of skidding and slipping in wheeled mobile robots: Control design perspective. J. IEEE Trans. on Automatic Control, vol.24, no. 3, pp.676–687, 2008.

[5] Shuang, G., Cheung, N., Cheng, E., Lei, D., Xiaozhong, L.:" Skid steering in 4WD EV. In: Proc. of 4th Int. Workshop on Robot and Motion Control, pp. 175–180, 2004.

[6] Low, C.B., Wang, D.:" Integrated estimation for wheeled mobile robot posture, velocities, and wheel skidding perturbations". In: IROS 2008 Workshop on Modeling, Estimation, Path Planning and Control of All Terrain Mobile Robots, pp. 20–30, 2008.

[7] Pazderski, D., Kozlowski, K.: "Trajectory tracking control of Skid-Steering Robot - experimental validation. In: Proc. of 17th World Congress, IFAC, pp. 5377–5382, 2008.

[8] Maclaurin, B.: "Comparing the steering performances of skid- and Ackermann steered vehicles",. J. of Automobile Engineering , vo.22, no.5, pp. 739–756, 2008.

[9] Shamah, B.: "Experimental comparison of skid steering vs. explicit steering for a wheeled mobile robot", Report of the Robotics Institute, Carnegie Mellon Univ, CMU-RI-TR-99-06, pp. 1–54, 1999.

[10] Okada, T., Abeer, M.Mahmoud, A., Botelho, W., Shimizu, T.: "Trajectory analysis of an independently driven wheeled robot and its experimental verification. In: Proc. 12th Int. Conf. on CLAWAR, pp. 781–790, 2009.

[11] Hadwich, V., Pfeiffer, F.: "The principle of virtual work in mechanical and electromechanical systems". Archive of Applied Mechanics vol.65, pp.390–400, 1995.

[12] Sakai, H.: "Friction and wear of tire". Tire Science and Technology (TSTCA) 25(1), 1997.